MATERIALS PHYSICS AND MECHANICS RESEARCH ARTICLE

Submitted: July 3, 2025 **Revised: June 1, 2026** **Accepted: June 30, 2026**

Effect of technology of thermoelectric BiSbTe alloys on structural, thermoelectric and mechanical properties

G.V. Demyanov [1]✉, S.N. Nemov [1], V.D. Andreeva [1], I.A. Shishov [1], V.V. Mishin [1], A.V. Povolotskiy [2], V.S. Mukhamedzyanov [1]

[1] Peter the Great St. Petersburg Polytechnic University, St. Petersburg, Russia

[2] St. Petersburg State University of Film and Television, St. Petersburg, Russia

✉ demyanov.g@bk.ru

ABSTRACT

The parameters of the main technologies for producing thermoelectric materials are considered: zone melting and extrusion. The structure and properties of samples of thermoelectric BiSbTe alloys obtained by zone melting and hot extrusion are compared to identify the dependencies. The analysis was carried out using methods of X-ray phase analysis, metallographic analysis, Raman spectroscopy, investigation of thermoelectric properties by the probe method, and mathematical modeling. The dependences of the thermal EMF distribution over the cross section are obtained, and the experimental dependences are analyzed. As a result, it was revealed that the samples obtained by hot extrusion have a heterogeneity of structure and properties across the sample section, which is associated with a stress-strain state due to the presence of significant friction forces on the surface of the contact of the material with the matrix. No such patterns were found for samples obtained by zone melting.

KEYWORDS

thermoelectricity • zone melting • extrusion • thermoelectric alloys • structure • mathematical modeling

Citation: Demyanov GV, Nemov SN, Andreeva VD, Shishov IA, Mishin VV, Povolotskiy AV, Mukhamedzyanov VS. Effect of technology of thermoelectric BiSbTe alloys on structural, thermoelectric and mechanical properties. *Materials Physics and Mechanics*. 2026;54(4): 98–107.
http://dx.doi.org/10.18149/MPM.5442026_9

Introduction

The utilization of thermoelectricity represents one of the most promising areas in alternative energy [1–5]. Materials based on antimony and bismuth chalcogenides enable the direct conversion of heat into electricity in accordance with the Seebeck, Peltier, and Thomson effects [6]. Moreover, this conversion process is characterized by a minimal environmental impact [7]. Additionally, thermoelectric materials are widely utilized in an industry for the design of refrigeration systems and for powering localized sensors [8,9]. Another significant advantage of thermoelectric materials is their high stability and resistance to external impacts. A prime example of this is radioisotope thermoelectric generators (RTGs), where the decay of a radioactive substance releases sufficient thermal energy to generate electricity for space applications and other equipment using Peltier elements [10–13].

However, the aforementioned advantages are accompanied by certain drawbacks of thermoelectric materials. These include their low efficiency, which is approximately 8 % [14,15]. At the same time, depending on the manufacturing technology, composition, and structure of the alloy, the efficiency can vary [16,17].

© G.V. Demyanov, S.N. Nemov, V.D. Andreeva, I.A. Shishov, V.V. Mishin, A.V. Povolotskiy, V.S. Mukhamedzyanov, 2026.
Publisher: Peter the Great St. Petersburg Polytechnic University
This is an open access article under the CC BY-NC 4.0 license (https://creativecommons.org/li-censes/by-nc/4.0/)

There are two approaches to increasing the efficiency of thermoelectric elements. The first approach is aimed at modifying and optimizing the chemical composition of the material and the addition of dopants. The essence of the second approach lies in the improvement of the manufacturing technologies and the material's structure [18,19].

Consequently, the task of studying the relationship between the structure and physical properties of BiSbTe alloys is of high relevance [20]. The obtained data will allow for the optimization of the manufacturing technology for thermoelectric elements, which, collectively, will lead to an increase in the thermoelectric efficiency of the devices.

The main industrial methods for producing thermoelectric materials are zone melting and hot extrusion [21,22]. In zone melting, the synthesis of compounds is carried out in evacuated quartz ampoules containing the pulverized components. Subsequently, as the hot zone moves, the recrystallization of the material occurs (purification of the substance based on the difference in solubility at various temperatures) [23]. Currently, an alternative technology for producing thermoelectric materials—hot extrusion—attracts greater interest. In this case, the material is pre-granulated, loaded into an extruder, and forced through a die [24–27].

The heterogeneity of the structural and thermoelectric properties across the cross-section of extruded BiSbTe alloys has been discussed in several studies [25,28,29]. These works describe the influence of friction forces, the stress-strain state, and temperature gradients on the formation of the material's texture. In [30,31], it was demonstrated that charge carrier mobility and the Seebeck coefficient strongly depend on the local structure and grain distribution, which are formed under the influence of friction and shear forces. A significant contribution to electron mobility is also made by the size and misorientation of crystallites [32]. As previous study [33] indicated, the properties and structure of the materials vary drastically depending on the distance from the center of the billet, both in terms of phase composition and thermo-EMF (termoelectric effect).

Materials and Methods

In this study, samples obtained by zone melting and hot extrusion are considered. Samples with the composition $Bi_xSb_{2-x}Te_3$ were produced using the extrusion method. The first stage of synthesis involves melting the components in a graphite crucible at a temperature of 700 °C. Subsequently, the resulting melt is atomized in an argon atmosphere. The average size of the obtained particles is 3 mm. The final step of this stage is cold pressing (material processing aimed at creating a specified shape under pressure without heating) to a density of 6 g/cm^3. The phase composition of the synthesized material at this stage was not investigated. Both extrusion and zone melting were performed using the same batch of the synthesized material.

The obtained billets were placed into an extruder, where, after preheating the tool and the billet to a temperature of 400 °C, the material was extruded at a rate of approximately 0.3 mm/min in an inert argon atmosphere. The extruded billets were not subjected to homogenizing annealing. The diameter of the extruded samples is 25.4 mm.

For zone melting, the initial components were placed in an evacuated quartz ampoule. During the melting process, the ampoule was continuously rotated to minimize material inhomogeneity. The growth rate was approximately 8 mm/min. The diameter of

the samples obtained by zone melting is 25.4 mm. Similar to the extruded billets, the ingots obtained by zone melting were not subjected to homogenizing annealing.

Next, the obtained billets and ingots were cut into cylindrical samples. To study the structure and establish property correlations, the following investigations were conducted in this work: analysis of the phase composition, Raman spectroscopy, metallography, thermo-EMF measurements, and finite element modeling of the extrusion process. X-ray diffraction (XRD) analysis was performed using a Bruker D8 Advance diffractometer. The phases were identified by comparing the obtained peaks with the International Centre for Diffraction Data (ICDD) database.

The hot-extruded samples were measured in three distinct regions, which were defined based on previous studies [33]. Zone 1 represents the surface layer of the billet (ring thickness of 2.5 mm). Zone 2 is the intermediate peripheral region (ring thickness of 6.0 mm), and Zone 3 is the central part of the sample (radius of 4.2 mm). The characteristic zones of the extruded sample are shown in Fig. 1. The total radius of the sample is 12.7 mm, and the dimensions of the specified zones strictly correspond to this value.

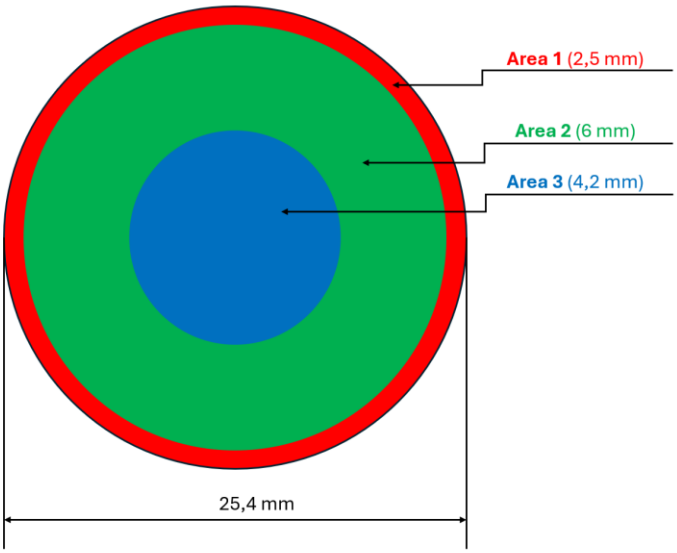


Fig. 1. Characteristic measurement areas of the extruded samples: Zone 1 represents the surface layer of the billet (ring thickness of 2.5 mm), Zone 3 is the central part of the sample (radius of 4.2 mm), and Zone 2 is the peripheral region of the billet (ring thickness of 6.0 mm)

The samples were examined on a spectrometer in a backscattering configuration excited by a laser with a wavelength of 63.8 nm and a power of 3 MW using a confocal microscope and microlenses with a magnification factor of 50. The diameter of the laser irradiation spot on the sample surface varied within 2 μm. Metallographic analysis of the extruded sample was carried out in three characteristic areas identified by the results of the analysis of the thermal EMF distribution. To analyze the effect of the stress-strain state during extrusion on the parameters of temoEDS, modeling was performed in the DEFORM software package. The rheological model and the stress strain state model are calculated based on open sources [25,28,34]. According to these models, the Young's modulus and Poisson's ratio are 40 GPa and 0.3, respectively. The elemental composition in the characteristic places of the ingot was determined in the center and in the extreme region of the sample using a Tescan MIRA 3 scanning electron microscope (SEM).

Results and Discussion

Phase composition

In previous studies, an inhomogeneous distribution of thermo-EMF over the cross-section of extruded rods was found [33]. In this regard, studies of the phase composition have been undertaken. X-ray phase analysis showed that the billet has a phase structure of variable composition based on solid solutions of antimony and bismuth telluride, close to $(Bi_{0,5}Sb_{1,5})\ Te_3$ (Fig. 2).

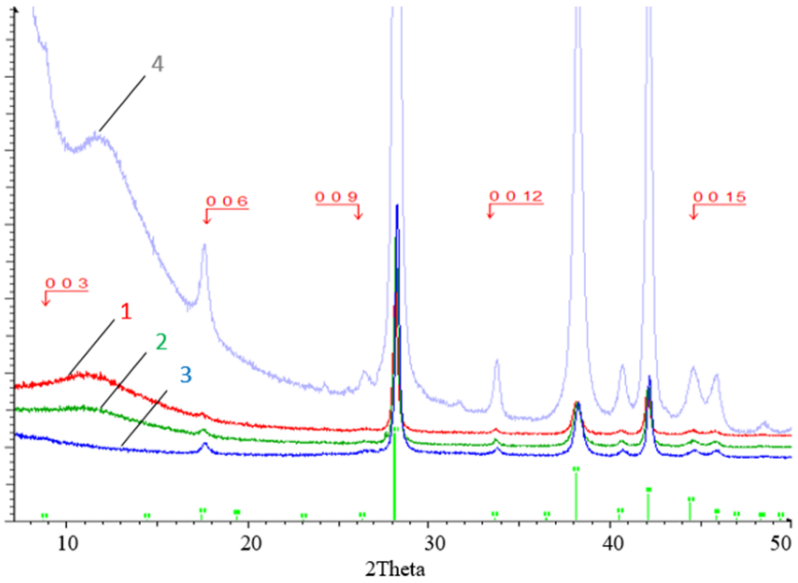


Fig. 2. X-ray diffraction patterns of the investigated areas ($\lambda_{CuK\alpha}$=1.54178 Å): 1 — lateral surface of the billet (Zone 1); 2 — peripheral region of the billet (Zone 2); 3 — central part of the sample (Zone 3); 4 — XRD pattern averaged over the entire cross-section of the billet

Phase distribution over the sample section

The lateral surface consists of almost 75 % of the X-ray amorphous phase. The ratio of the components of the crystalline component of antimony and bismuth telluride is consistent with the structural parameters $Bi_{0.3}Sb_{1.7}Te_3$. As the distance from the surface of the workpiece increases, the proportion of Bi increases. The following reflexes appear: $Bi_{1.5}Sb_{0.5}Te_3$. The proportion of the amorphous component decreases. Traces of the Bi_8Te_9 phase, which has a lower crystallization temperature, are also observed. There is no amorphous phase in the central area of the workpiece. The phase with the Bi_8Te_9 structure is also present in insignificant amounts. The base is $Bi_{0.3}Sb_{1.7}Te_3$ with some $Bi_{1.5}Sb_{0.5}Te_3$. The composition of the solid solution is close to the ratio Sb_2Te_3/Bi_2Te_3=65 %/35 %.

To correlate the thermopower values with the character of the crystallite orientation distribution over the ingot section, a series of surveys was carried out with discrete rotation of the sample (φ = 0–360°) around the axis of the ingot growth direction coinciding with the direction of 110 rhombohedral crystals (Fig. 3).

Polar diagrams were constructed showing the peak intensities of 110 (2Θ about 42°) and 00.15 (2Θ ≈ 45°) in the surface and central cross-sectional areas of the workpiece.

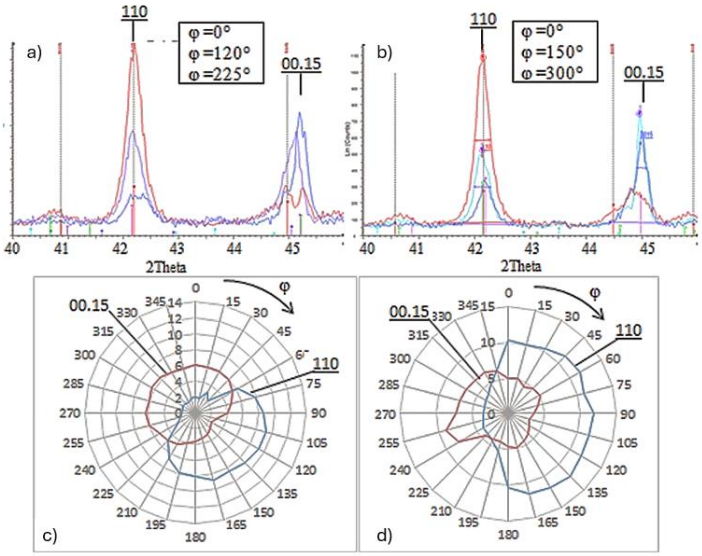
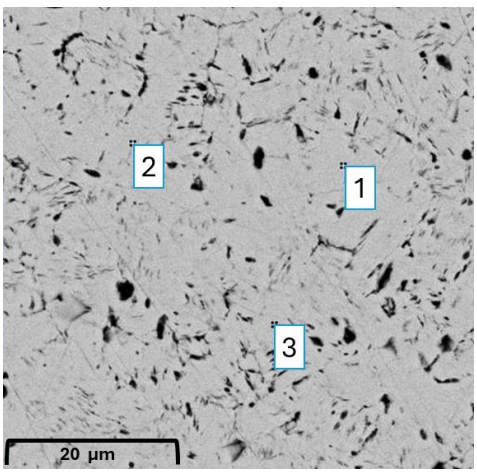
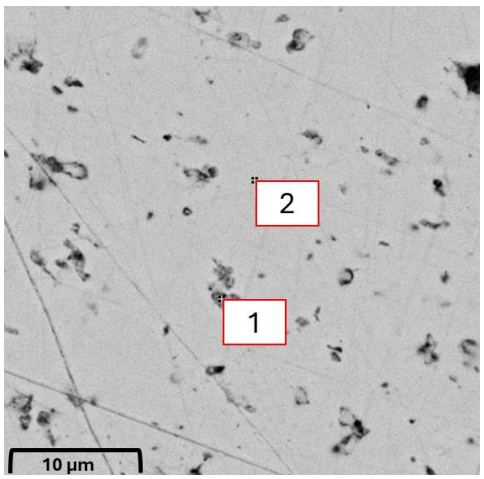


Fig. 3. X-ray sections and an illustration of the nature of textural scattering of zone 1 (a,c) and zone 3 (b,d), respectively

The misorientation of crystals in the 00.15 plane is insignificant and, on average, does not exceed 4–6° over the entire cross-section, while the variation of deviations of the direction [110] from the axis of the workpiece ranges from 2 to 8° along the edge of the sample (area 1) and reaches 12° in the central regions. An analysis of the peak widenings showed that the structure in the lateral region (area 1) is more dispersed than in the central zone. Thus, the broadening of peak 110 in zone 1 reaches 0.30–0.55°. There is a 0.3° broadening in the center of the workpiece. A uniform composition of the solid solution was observed across the entire investigated surface, with the atomic fraction of Bi approximately equal to 0.43–0.44 at. (Fig. 4). An electron microscopic analysis was also performed for the ingot edge (area 1). The results are presented in Table 1 and 2, and Fig. 4.



1. $Bi_{0.43}\ Sb_{1.59}\ Te_{2,96}$
2. $Bi_{0.43}\ Sb_{1.59}\ Te_{2,98}$
3. $Bi_{0.44}\ Sb_{1.61}\ Te_{2,94}$



1. $Bi_{0.42}\ Sb_{1.58}\ Te_3$
2. $Bi_{0.44}\ Sb_{1.60}\ Te_{2.96}$

Fig. 4. The structure of the extruded sample in the back-reflected electron (BSE) mode: (a) the central region (area 3); (b) the edge of the ingot (area 1)

Table 1. The elemental composition of the ingot in the central zone

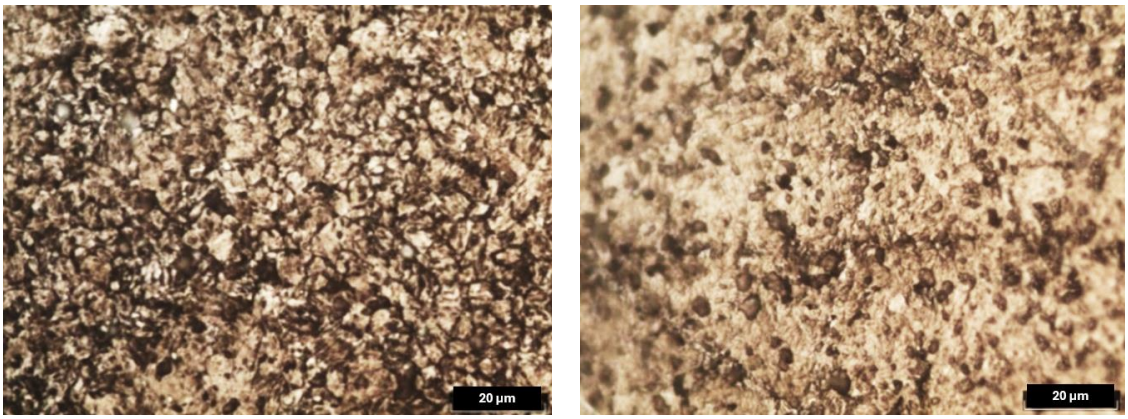
Spectrum	Sb	Te	Bi
1	31.99	59.34	8.67
2	31.86	59.65	8.49
3	32.28	58.79	8.92
Average	32.04	59.26	8.7
Standard. deviation	0.22	0.43	0.22
Max.	32.28	59.65	8.92
Min.	31.86	58.79	8.49

Table 2. The elemental composition of the ingot edge

Spectrum	Sb	Te	Bi
Spectrum 1	31.68	59.82	8.50
Spectrum 2	32.11	59.12	8.77
Average	31.90	59.47	8.64
Standard. deviation	0.30	0.50	0.20
Max.	32.11	59.82	8.77
Min.	31.68	59.12	8.50

Regions exhibiting dark contrast were depleted in Bi (0.42 at. % compared to the average 0.44 at. %). Conversely, regions with light contrast were enriched in Bi (0.46 at. % vs. the nominal 0.44 at. %). The composition of the amorphous phase was found to be close to that of the crystalline matrix in the central region of the ingot – $Bi_{0.44}Sb_{1.61}Te_{2.95}$. However, some areas are less rich in Bi (spectrum 1 in Fig. 4– $Bi_{0.42}Sb_{1.58}Te_3$ – size of 0.5–2.0 μm), individual crystals with a size of 2 μm (point 2) and 5 μm (point 1) are also clearly visible, containing more Bi – $Bi_{0.46}Sb_{1.56}Te_{2.96}$.

Figure 5 shows the structure of the extruded sample in the central zone and at the edge of the ingot (area 1). Angular crystalline grains of 3–10 μm in size can be observed on it. Based on the analysis of metallographic photographs of the central area of the workpiece (area 3), there is no amorphous phase. A slight broadening of the peaks is observed in the RAMAN spectra (Fig. 6). This may be due to the heterogeneity of the chemical composition and the presence of stress. It is clearly seen that the bands 107 and 158 cm^{-1} are decreasing, and the bands in the area 117 and 138 cm^{-1} are growing. The lines widen as they move towards the edge of the ingot, that is, deformations increase from the center to the edge.



(a) (b)

Fig. 5. The structure of the extruded sample obtained on an optical microscope: (a) in the central zone (area 3); (b) the edges of the ingot (area 1)

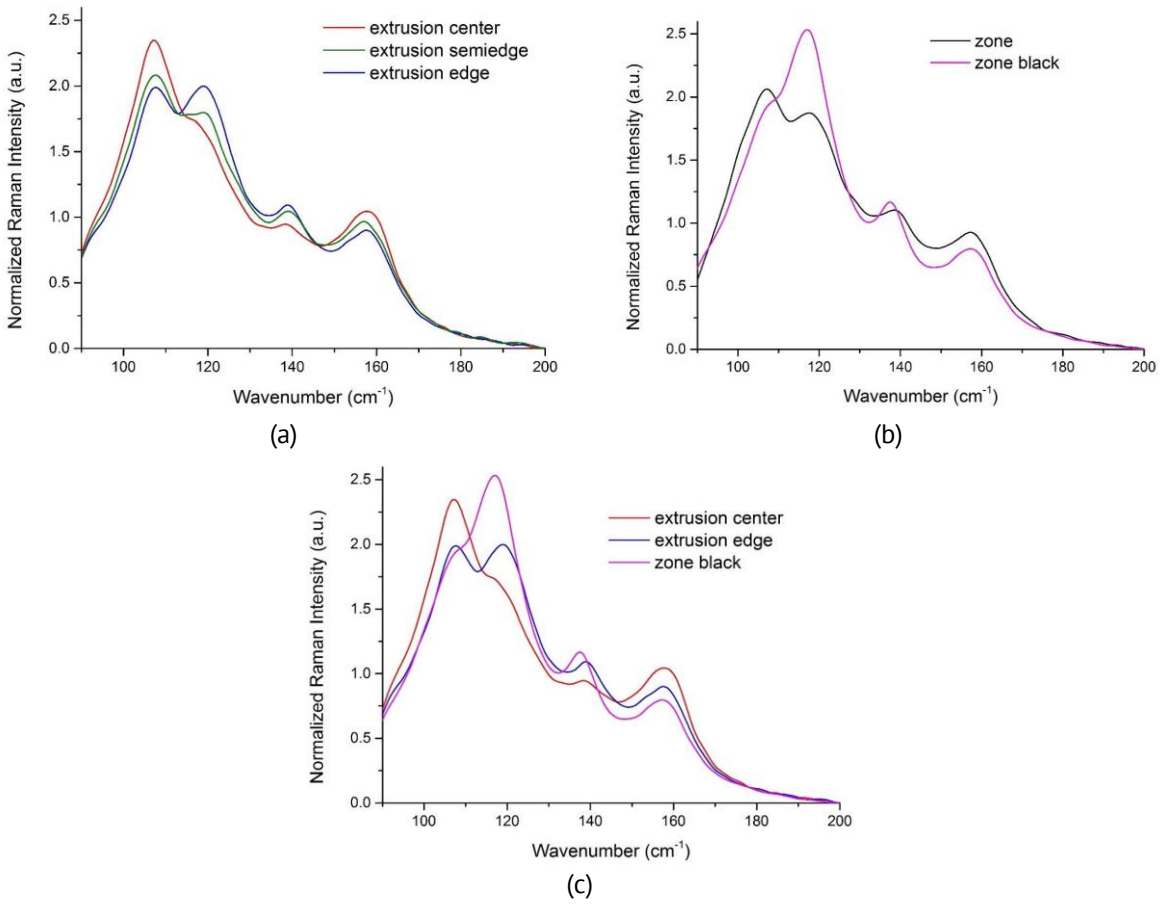


Fig. 6. Raman spectra: (a) spectra of RAMAN (Bi_xSb_{2-x}) Te_3 produced by extrusion: the red line is the center of the sample, the green line is the intermediate region, the blue line is the edge of the sample; (b) Raman spectra (Bi_xSb_{2-x}) Te_3 produced by zone melting; (c) combined RAMAN spectra (Bi_xSb_{2-x}) Te_3

This may be due to metal leakage during the extrusion process. Due to friction forces, shear deformations occur, and the lines widen. A similar stress-strain state in various areas was established in [34] using mathematical modeling of the process of hot extrusion of thermoelectric materials.

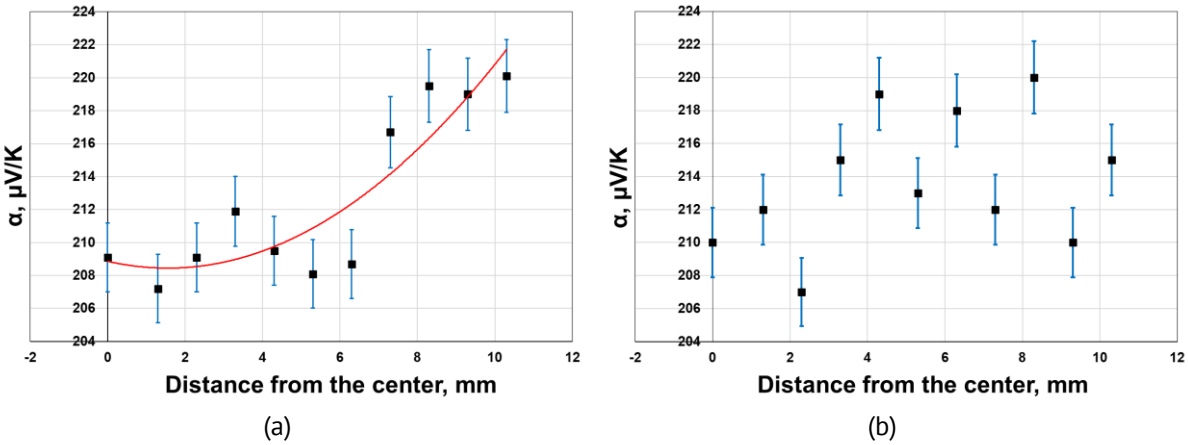


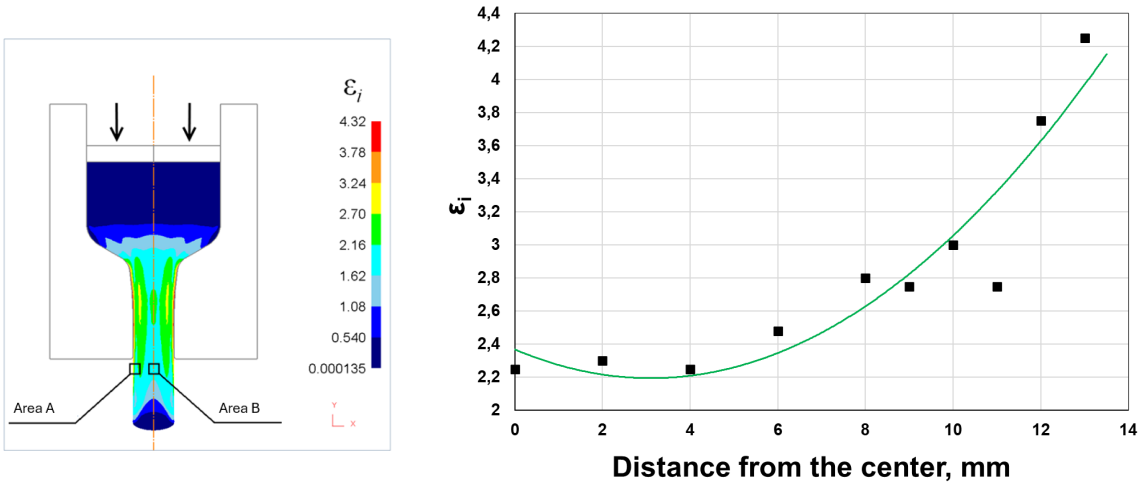
Fig. 7. Distribution of the thermo-EMF in the billet: (a) in the extruded billet at the die exit as a function of the distance from the center (the solid line represents a second-degree polynomial approximation; error bars correspond to a 1 % confidence interval); (b) in the billet obtained by zone melting as a function of the distance from the center

To evaluate the distribution profile of the thermo-EMF across the sample cross-section, probe-based measurements were conducted. The measurements were carried out on a polycrystalline sample along its diameter with a step of 1.3 mm. Based on the probe testing results, the radial dependence of the thermo-EMF on the distance from the center was plotted (Fig. 7).

The behavior of the dependence for the extruded rods and the samples obtained by zone melting differs significantly. For the extruded samples, the thermo-EMF distribution is described by a second-degree polynomial (a parabola), exhibiting an increase from the central part of the billet toward its periphery. In contrast, for the zone-melted samples, the Seebeck coefficient values exhibit a random distribution.

Extrusion modeling in DEFORM

A simulation of the billet extrusion process using the finite element method in the DEFORM program has been performed. Of the greatest interest is the analysis of the distribution of the accumulated intensity of plastic deformation ε_i in the workpiece at the exit from the matrix (Fig. 8).



(a) (b)

Fig. 8. Distributions of the accumulated intensity of plastic deformation: (a) ε_i in the workpiece at the exit from the matrix; (b) ε_i values at the exit from the deformation site

It is clearly observed that the accumulated effective strain (ε_i) exhibits a highly heterogeneous distribution both within the deformation zone and at the die exit. Specifically, the ε_i values in the central region of the extruded rod are approximately half those measured near the ingot surface. This strain distribution pattern arises from elevated shear stresses and strains within the surface layers of the ingot, resulting from significant frictional forces at the rod/tooling interface.

The dependence profiles of the accumulated equivalent strain, ε_i, and the thermo-EMF distribution are monotonic and exhibit similar trends. This correlation allows us to conclude that the inhomogeneous distribution of the stress-strain state directly influences the thermo-EMF distribution. In contrast, no such monotonic distribution of the thermo-EMF was observed for the zone-melted samples.

Conclusions

Thus, the structure of the extruded rod exhibits an inhomogeneous distribution of the thermo-EMF across its cross-section, which is attributed to the inhomogeneity of the stress-strain state and the misorientation of crystallites. Such a variation in the properties of thermoelectric materials across the billet may indicate imperfections in the manufacturing technology. In the samples obtained by zone melting, no such dependence was observed.

CRediT authorship contribution statement

Gregory V. Demyanov: writing – review & editing, writing – original draft; **Sergey N. Nemov**: conceptualization; **Valentina D. Andreeva**: data curation; **Ivan A. Shishov**: data curation; **Vasiliy V. Mishin**: data curation; **Alexey V. Povolotskiy**: supervision; **Vladimir S. Mukhamedzyanov**: investigation.

Conflict of interest

The authors declare that they have no conflict of interest.

References

1. Shoeibi S, Kargarsharifabad H, Sadi M, Arabkoohsar A, Mirjalily SAA. A review on using thermoelectric cooling, heating, and electricity generators in solar energy applications. *Sustainable Energy Technologies and Assessments.* 2022;52: 102105.
2. Wehbi Z, Taher R, Faraj J, Castelain C, Khaled M. Hybrid thermoelectric generators-renewable energy systems: A short review on recent developments. *Energy Reports.* 2022;8: 1361–1370.
3. Zheng XF, Liu CX, Yan YY, Wang Q. A review of thermoelectrics research–Recent developments and potentials for sustainable and renewable energy applications. *Renewable and Sustainable Energy Reviews.* 2014;32: 486–503.
4. Hendy MH, El-Attar SI, Ezzat MA. Thermoelectric viscoelastic spherical cavity with memory-dependent derivative. *Materials Physics and Mechanics.* 2021;47(2): 170–185.
5. Gribanov EN, Markov OI, Khripunov YuV. Quantum-chemical modeling of bismuth-based clusters. *Materials Physics and Mechanics.* 2020;43(1): 72–83.
6. He J, Hu X, Liu Z, Chen W, Longo G. Prospect for Bismuth/Antimony Chalcohalides-Based Solar Cells. *Advanced Functional Materials.* 2023;33(48): 2306075.
7. Caballero-Calero O, Ares JR, Martín-González M. Environmentally friendly thermoelectric materials: high performance from inorganic components with low toxicity and abundance in the earth. *Advanced Sustainable Systems.* 2021;5(11): 2100095.
8. Siddique ARM, Bozorgi M, Venkateshwar K, Tasnim S, Mahmud S. Phase change material-enhanced solid-state thermoelectric cooling technology for food refrigeration and storage applications. *Journal of Energy Storage.* 2023;60: 106569.
9. Xie H, Zhang Y, Gao P. Thermoelectric-powered sensors for Internet of Things. *Micromachines.* 2022;14(1): 31.
10. O'brien RC, Ambrosi RM, Bannister NP, Howe SD, Atkinson HV. Safe radioisotope thermoelectric generators and heat sources for space applications. *Journal of Nuclear Materials.* 2008;377(3): 506–521.
11. Wang C, Xu Z, Wang H, Cai T, Tao H, Wang Y, Tang X. Combined energy supply and management of self-powered wireless sensors based on radioisotope thermoelectric generator for multiple scenarios. *Energy Conversion and Management.* 2023;297: 117706.
12. Candolfi C, El Oualid S, Lenoir B, Caillat T. Progress and perspectives in thermoelectric generators for waste-heat recovery and space applications. *Journal of Applied Physics.* 2023;134(10): 100901.

13. Candolfi C, Oualid SE, Ibrahim D, Misra S, Hamouli OE, Léon A, Dauscher A, Masschelein P, Gall P, Gougeon P, Semprimoschnig C, Lenoir B. Thermoelectric materials for space applications. *CEAS Space Journal.* 2021;13: 325–340.
14. Gaurav K, Pandey SK. Efficiency calculation of a thermoelectric generator for investigating the applicability of various thermoelectric materials. *Journal of Renewable and Sustainable Energy.* 2017;9(1): 014701.
15. Twaha S, Zhu J, Yan Y, Li B. A comprehensive review of thermoelectric technology: Materials, applications, modelling and performance improvement. *Renewable and Sustainable Energy Reviews.* 2016;65: 698–726.
16. Tan G, Zhao LD, Kanatzidis MG. Rationally designing high-performance bulk thermoelectric materials. *Chemical Reviews.* 2016;116(19): 12123–12149.
17. Shi XL, Zou J, Chen ZG. Advanced thermoelectric design: from materials and structures to devices. *Chemical Reviews.* 2020;120(15): 7399–7515.
18. Han H, Zhao L, Wu X, Zuo B, Bian S, Li T, Liu X, Jiang Y, Chen C, Bi J, Xu J, Yu L. Advancements in thermoelectric materials: optimization strategies for enhancing energy conversion. *Journal of Materials Chemistry A.* 2024;12(36): 24041–24083.
19. Shtern Y, Sherchenkov A, Shtern M, Rogachev M, Pepelyaev D. Challenges and perspective recent trends of enhancing the efficiency of thermoelectric materials on the basis of PbTe. *Materials Today Communications.* 2023;37: 107083.
20. Zhao P, Yu F, Wang B, Zhao H, Chen C, Wang D, Ying P, Wu Y, Li P, Zhang B, Liu B, Zhao Z, Hu W, Yu D, He J, Liu Z, Xu B, Tian Y. Porous bismuth antimony telluride alloys with excellent thermoelectric and mechanical properties. *Journal of Materials Chemistry A.* 2021;9(8): 4990–4999.
21. Lu T, Wang B, Li G, Yang J, Zhang X, Chen N, Liu TH, Yang R, Niu P, Kan Z, Zhu H, Zhao H. Synergistically enhanced thermoelectric and mechanical performance of Bi_2Te_3 via industrial scalable hot extrusion method for cooling and power generation applications. *Materials Today Physics.* 2023;32: 101035.
22. d'Angelo M, Galassi C, Lecis N. Thermoelectric materials and applications: A review. *Energies.* 2023;16(17): 6409.
23. Xia H, Li X, Xu Q. Macro-Micro-Coupling Simulation and Space Experiment Study on Zone Melting Process of Bismuth Telluride-Based Crystal Materials. *Metals.* 2022;12(5): 886.
24. Zhang Y, Xu G, Nozariasbmarz A, Li W, Raman L, Xing C, Sharma S, Liu N, Ghosh S, Joshi G, Sanghadasa M, Shashank P, Poudel B. Thermoelectric cooling performance enhancement in BiSeTe alloy by microstructure modulation via hot extrusion. *Small Science.* 2024;4(2): 2300245.
25. MG Lavrentev, VT Bublik, FO Milovich, VP Panchenko, YN Parkhomenko, AI Prostomolotov, Tabachkova NYu, Verezub NA, Voronov MV, Yarkov Ivan Yu. Regularities of structure formation in 30 mm rods of thermoelectric material during hot extrusion. *Materials.* 2021;14(22): 7059.
26. Lavrentev M. G, VP Panchenko, YN Parkhomenko, AS Prosviryakov, NY Tabachkova, M.V. Voronov. Effect of Grain Size Distribution in Raw Powders on the Thermoelectric and Mechanical Properties of Hot-Extruded $Bi_{0.4}Sb_{1.6}Te_3$ and $Bi_2Te_{2.85}Se_{0.15}$ Solid Solutions. *Solid State Sciences.* 2025;161: 107858.
27. Zhao L, Zhang H, Zhao D, Wang D, Liu R, Feng J. High Mechanical Property and Texture Degree of Hot-Extruded Bi0.905Sb0.095. *Crystals.* 2024;14(6): 557.
28. Lavrentyev MG, Osvenskiy VB, Mezhennyy MV, Prostomolotov AI, Bublik VT, Tabachkova NY. Experiment-calculated study on structure formation of thermoelectric material based on solid solutions of bismuth and antimony chalcogenides prepared by hot extrusion method. *Journal of Thermoelectricity.* 2012;4: 33–38.
29. Sokolov OB, Skipidarov SY, Duvankov NI. Some peculiar features of plastic deformation and diffusion processes in hot extrusions of n-Bi2(Te, Se)3 and p-(Bi, Sb)2Te3. *Journal of Thermoelectricity.* 2004;1: 48–54.
30. Wang ZL, Araki T, Onda T, Chen ZC. Effect of annealing on microstructure and thermoelectric properties of hot-extruded Bi–Sb–Te bulk materials. *Journal of Materials Science.* 2018;53(12): 9117–9130.
31. Yang J, Chen R, Fan X, Zhu W, Bao S, Duan X. Microstructure control and thermoelectric properties improvement to n-type bismuth telluride based materials by hot extrusion. *Journal of Alloys and Compounds.* 2007;429(1–2): 156–162.
32. Gayner C, Natanzon Y, Kauffmann Y, Amouyal Y. Topologically-enhanced thermoelectric properties in Bi_2Te_3-based compounds: Effects of grain size and misorientation. *ACS Applied Materials & Interfaces.* 2022;14(44): 49730–49745.
33. Nemov SA, Andreeva VD, Maslikova EI, Mishin VV, Shishov IA, Demyanov GV. Features of the structure of thermoelectric samples obtained by extrusion. In: *Proc. the International Symposium for Nanophysics and Nanomaterials.* Saint Petersburg Mining University: St. Petersburg; 2021. p.196–201. (In Russian)
34. Lavrentyev MG, Mezhennyy MV, Osvenskiy VB, Prostomolotov AI. Mathematical modeling of the extrusion process of thermoelectric material. *Materials of Electronic Engineering.* 2012;3: 35–40. (In Russian)